

Collective Dissipation and Parameter Sensitivity in Trapped Ions Coupled to a Common Thermal Reservoir

C. F. P. Avalos,^{1,*} G. A. Prataviera,^{2,†} and M. C. de Oliveira^{1,‡}

¹*Instituto de Física Gleb Wataghin, Universidade Estadual de Campinas, 13083-859, Campinas, SP, Brazil*

²*Departamento de Administração, FEA-RP, Universidade de São Paulo, 14040-905, Ribeirão Preto, SP, Brazil*

(Dated: December 23, 2025)

We investigate the dynamics of two trapped ions interacting with a common thermal reservoir, focusing on how cross-correlated dissipation influences heating, steady-state behavior, and parameter sensitivity. Starting from a microscopic system-reservoir model, we derive the corresponding Heisenberg-Langevin equations and show that reservoir-induced correlations generate collective decay channels and, when the cross-damping rate matches the local damping, a decoherence-free normal mode that preserves memory of the initial excitations. Using the Fisher information associated with motional population measurements, we identify the parameter regimes in which cross-damping enhances the estimability of both system and reservoir properties. For non-classical initial states, we also show that reservoir-mediated correlations can generate or maintain entanglement, with the strongest effects occurring near the decoherence-free condition.

I. INTRODUCTION

Trapped ions are among the most versatile and precisely controllable platforms for quantum information processing, quantum simulation, and precision metrology [1–3]. Their internal electronic states can be addressed with high fidelity, and their quantized motional modes offer long coherence times and flexible engineering of interactions. These features have enabled state-of-the-art demonstrations in quantum logic, entanglement generation, and ultra-sensitive force and field sensing.

Despite this high degree of control, trapped-ion performance remains limited by motional heating and decoherence. Fluctuating electromagnetic fields near trap surfaces, technical noise, and coupling to uncontrolled environmental degrees of freedom can inject energy into the motional modes, degrade nonclassical resources, and ultimately constrain gate fidelity and metrological sensitivity [3, 4]. In the standard description, each ion interacts with an effectively independent reservoir, so dissipation acts locally with motional states relaxing individually through independent decay channels towards thermal equilibrium, suppressing coherence, squeezing, and entanglement.

In many experimental architectures, however, ions do not couple to independent noise sources. Shared trap electrodes, common voltage supplies, and the finite correlation length of fluctuating surface potentials lead to situations in which environmental fluctuations are at least partially correlated across the ion array. In this collective-dissipation regime, cross-damping terms modify the relaxation dynamics and give rise to qualitatively new phenomena. These include superradiant and subradiant decay channels, modified steady-state occupations, and the possibility of a decoherence-free subspace (DFS) when the cross-damping rate matches the local damping [5–7]. Moreover, a common reservoir can mediate correlations or even generate entanglement between otherwise uncoupled degrees of freedom, as shown for both two-level systems [5, 6, 8, 9] and bosonic modes [7, 10–12].

Although these effects are well documented individually, a unified analysis that connects a microscopically derived cross-damped Langevin description with quantitative measures of parameter sensitivity and entanglement remains largely unexplored. The present work aims to provide such a comprehensive treatment for two Coulomb-coupled trapped ions interacting with a shared thermal reservoir. Our approach combines a fully analytic derivation of the dissipative normal modes with an information-theoretic analysis of estimability and a Gaussian-state entanglement study. Related analyses of non-classical motional dynamics in trapped-ion systems have been developed in the unitary, non-adiabatic regime, where squeezing and P-nonclassicality emerge as resources for quantum thermodynamics and sensing [13].

Beyond consolidating established aspects of collective decay and decoherence-free subspaces, our work advances the field in three key directions. First, we provide a microscopic and fully analytic treatment of cross-damped Langevin dynamics for Coulomb-coupled ions, enabling an exact identification of collective decay channels and their dependence on reservoir correlations. Second, we connect this dynamical structure to information-theoretic performance by computing the full classical Fisher information matrix for experimentally accessible phonon-number measurements. This reveals how correlated dissipation can enhance or even preserve the estimability of system and reservoir parameters—an aspect not addressed in previous analyses of trapped-ion thermometry or collective damping. Third, we demonstrate that the same mechanism that enhances metrological performance also governs the creation and persistence of Gaussian entanglement, providing a unified physical picture of how

* cfavalos@ifi.unicamp.br

† prataviera@usp.br

‡ marcos@ifi.unicamp.br

reservoir correlations act simultaneously as a generator and stabilizer of nonclassical motional states. These results establish collective dissipation not only as a decoherence mechanism but as a tunable resource for precision sensing and quantum-state engineering in trapped-ion platforms.

The paper is organized as follows. Section II presents the two-ion Hamiltonian and summarizes the approximations used. Section III introduces the interaction with a common thermal reservoir and derives the corresponding Heisenberg–Langevin equations. Section IV analyzes the resulting dynamics, including collective decay rates, heating behavior, and the emergence of a decoherence-free subspace. In Sec. V we compute the Fisher information for population measurements and discuss the distinct estimation regimes that emerge for different correlation strengths. Section VI examines the entanglement dynamics of nonclassical initial states under collective dissipation. Our conclusions are presented in Sec. VII.

II. TWO-ION SYSTEM

We consider two ions of mass m and charge q confined in a linear Paul trap and separated by a distance d . The ions oscillate around their equilibrium positions and interact through the Coulomb repulsion. We focus on the longitudinal motional degree of freedom along the ion–ion axis, for which the system Hamiltonian can be written as [1–3]

$$H = \sum_{j=1}^2 \left(\frac{p_j^2}{2m} + \frac{1}{2}m\omega^2 x_j^2 \right) + H_C, \quad (1)$$

where ω is the trapping frequency, and

$$H_C = \frac{kq^2}{d + x_2 - x_1}, \quad (2)$$

with $k = (4\pi\epsilon_0)^{-1}$.

For small displacements, $|x_2 - x_1| \ll d$, we expand Eq. (2) to second order as

$$H_C \approx \frac{kq^2}{d} \left[1 - \frac{x_2 - x_1}{d} + \frac{(x_2 - x_1)^2}{d^2} \right]. \quad (3)$$

In Eq. 3, the constant term contributes only an overall energy offset and can be ignored, while the linear term merely shifts the equilibrium positions and the quadratic terms modify the trap frequency and generate an effective bilinear coupling between the ions.

Introducing bosonic operators

$$x_j = \sqrt{\frac{\hbar}{2m\omega}}(a_j + a_j^\dagger), \quad p_j = i\sqrt{\frac{\hbar m\omega}{2}}(a_j^\dagger - a_j), \quad (4)$$

the Hamiltonian becomes

$$\begin{aligned} H = & \hbar\omega_0(a_1^\dagger a_1 + a_2^\dagger a_2) + \sqrt{\frac{\hbar k^2 q^4}{2m\omega d^4}}(a_1 + a_1^\dagger - a_2 - a_2^\dagger) \\ & + \frac{\hbar k q^2}{2m\omega d^3} \left(a_1^2 + a_1^{\dagger 2} + a_2^2 + a_2^{\dagger 2} \right) \\ & - \frac{\hbar k q^2}{m\omega d^3} \left(a_1 a_2^\dagger + a_2 a_1^\dagger + a_1 a_2 + a_1^\dagger a_2^\dagger \right), \end{aligned} \quad (5)$$

where $\omega_0 = \omega + kq^2/(m\omega d^3)$ are the renormalized ions frequencies, which includes the small frequency shift due to the Coulomb interaction.

Moving to the interaction picture with respect to

$$H_0 = \hbar\omega_0(a_1^\dagger a_1 + a_2^\dagger a_2),$$

and applying the rotating-wave approximation to neglect terms oscillating at $\pm\omega_0$, and $\pm 2\omega_0$ (which average out on the timescales of interest), we are left with the dominant bilinear coupling

$$\tilde{H} = \hbar\Omega \left(a_1 a_2^\dagger + a_1^\dagger a_2 \right), \quad (6)$$

where $\Omega = -kq^2/(m\omega d^3)$ is the effective coupling strength.

Equation (6) describes a beam-splitter-type interaction between the motional modes. Such a Hamiltonian does not generate entanglement from classical initial states, but can generate or exchange entanglement when at least one of the initial states is nonclassical. In the absence of environmental coupling, the dynamics are fully coherent and consist of periodic energy exchange between the two ions. As we show in the next section, coupling to a common environment qualitatively modifies this behavior through the appearance of cross-damping terms, which play a central role in the emergence of collective decay and decoherence-free subspaces.

III. DAMPING AND HEATING

We now incorporate dissipation by coupling the ions to a common thermal reservoir. The environment is modeled as a collection of bosonic modes with frequencies ω_k , which couple linearly to the motional annihilation operators of both ions. The full Hamiltonian reads

$$H = \sum_{j=1}^2 \hbar\omega_0 a_j^\dagger a_j + \hbar\Omega \left(a_1 a_2^\dagger + a_1^\dagger a_2 \right) + \sum_k \hbar\omega_k b_k^\dagger b_k + \sum_{j=1}^2 \sum_k \hbar \left(g_{jk} b_k a_j^\dagger + g_{jk}^* b_k^\dagger a_j \right), \quad (7)$$

where g_{jk} denotes the coupling strength between ion j and bath mode k , and the zero-point energies have been omitted, as they only add a constant shift to the Hamiltonian and do not affect the dynamics. The operators a_j and b_k annihilate excitations of the ions and the reservoir, respectively

The Heisenberg equations of motion are

$$\dot{a}_j = -i\omega_0 a_j - i\Omega a_l - i \sum_k g_{jk} b_k, \quad (8)$$

$$\dot{b}_k = -i\omega_k b_k - i \sum_{j=1}^2 g_{jk}^* a_j, \quad (9)$$

with $j \neq l = 1, 2$. Solving Eq. (9) formally and substituting into Eq. (8) yields

$$\begin{aligned} \dot{a}_j = & -i\omega_0 a_j - i\Omega a_l - i \sum_k g_{jk} b_k(0) e^{-i\omega_k t} \\ & - \sum_k |g_{jk}|^2 \int_0^t d\tau a_j(t-\tau) e^{-i\omega_k \tau} \\ & - \sum_k g_{jk} g_{lk}^* \int_0^t d\tau a_l(t-\tau) e^{-i\omega_k \tau}. \end{aligned} \quad (10)$$

The first two terms describe the system's coherent dynamics. The third term defines a noise operator,

$$F_j(t) = -i \sum_k g_{jk} b_k(0) e^{-i\omega_k t}, \quad (11)$$

while the last two terms represent dissipation generated by the reservoir. To evaluate these integrals, we replace the discrete sum over bath modes by a continuous distribution with density $\eta_{jl}(\omega)$ and define the cross spectral density

$$W_{jl}(\omega) = \eta_{jl}(\omega) g_j(\omega) g_l^*(\omega), \quad (12)$$

which satisfies [4]

$$W_{jl} = W_{lj}^*, \quad |W_{jl}| \leq \sqrt{W_{jj} W_{ll}}. \quad (13)$$

The generalized Wiener–Khinchin theorem gives the reservoir autocorrelation function

$$\Gamma_{jl}(\tau) = \int_{-\omega_0}^{\infty} W_{jl}(\omega_0 + \omega') e^{-i\omega' \tau} d\omega'. \quad (14)$$

Under the Markov approximation, $W_{jl}(\omega)$ varies slowly around ω_0 so that $W_{jl}(\omega_0 + \omega') \approx W_{jl}(\omega_0)$, yielding

$$\Gamma_{jl}(\tau) = 2\pi W_{jl}(\omega_0)\delta(\tau). \quad (15)$$

Inserting this into Eq. (10) gives the dissipative contribution

$$\sum_k g_{jk} g_{lk}^* \int_0^t a_l(t - \tau) e^{-i\omega_k \tau} d\tau \rightarrow \frac{\gamma_{jl}}{2} a_l(t), \quad (16)$$

where the damping rates are

$$\gamma_{jl} = 2\pi\eta_{jl}(\omega_0)g_j(\omega_0)g_l^*(\omega_0). \quad (17)$$

The Cauchy–Schwarz inequality implies

$$\gamma_{jl} \leq \sqrt{\gamma_{jj}\gamma_{ll}}, \quad (18)$$

showing that the cross-damping cannot exceed the local dissipation.

The noise operators satisfy, for a bath with mean thermal occupation \bar{N} ,

$$\langle F_j(t) \rangle = 0, \quad (19)$$

$$\langle F_j(t) F_l(t') \rangle = 0, \quad (20)$$

$$\langle F_j^\dagger(t) F_l(t') \rangle = \bar{N} \gamma_{jl} \delta(t - t'), \quad (21)$$

$$\langle F_j(t) F_l^\dagger(t') \rangle = (\bar{N} + 1) \gamma_{jl} \delta(t - t'). \quad (22)$$

Collecting all terms, we obtain the Heisenberg–Langevin equations

$$\dot{a}_j(t) = - \left(i\omega_0 + \frac{\gamma_{jj}}{2} \right) a_j(t) - \left(i\Omega + \frac{\gamma_{jl}}{2} \right) a_l(t) + F_j(t), \quad (23)$$

for $j, l = 1, 2$, showing that the common reservoir induces not only local damping γ_{jj} but also cross-damping γ_{jl} . The latter term arises from interference between decay channels and is responsible for the collective dynamics discussed in the next section.

IV. DYNAMICS AND EQUILIBRIUM

The Heisenberg–Langevin equations obtained in Sec. III describe the coupled dynamics of the ions under both coherent tunneling and dissipative interactions with the common reservoir. To analyze these equations, we first consider the general case without imposing any symmetry on the damping matrix, and only afterwards apply the physically motivated assumption that the ions are identical and couple equivalently to the bath.

Introducing the vector $\hat{\mathbf{a}} = (\hat{a}_1, \hat{a}_2)^T$ and the Langevin noise vector, $\mathbf{F}(t) = (F_1(t) F_2(t))^T$, the equations of motion can be written as

$$\dot{\hat{\mathbf{a}}}(t) = -i\mathbf{M}\hat{\mathbf{a}}(t) + \mathbf{F}(t), \quad (24)$$

where the drift matrix

$$\mathbf{M} = \begin{pmatrix} \omega_0 - i\gamma_{11}/2 & \Omega - i\gamma_{12}/2 \\ \Omega - i\gamma_{21}/2 & \omega_0 - i\gamma_{22}/2 \end{pmatrix} \quad (25)$$

contains both the coherent coupling Ω and all dissipative channels. The formal solution of Eq. (24) is

$$\hat{\mathbf{a}}(t) = e^{-i\mathbf{M}t} \hat{\mathbf{a}}(0) + \int_0^t e^{-i\mathbf{M}(t-t')} \mathbf{F}(t') dt'. \quad (26)$$

The matrix exponential $e^{-i\mathbf{M}t}$ can be expressed analytically by diagonalizing \mathbf{M} . The eigenvalues are

$$\lambda_{\pm} = \omega_0 - i \frac{\gamma_{11} + \gamma_{22}}{4} \pm \sqrt{\Delta}, \quad (27)$$

with

$$\Delta = \left(\Omega - i \frac{\gamma_{12}}{2} \right) \left(\Omega - i \frac{\gamma_{21}}{2} \right) - \left(\frac{\gamma_{11} - \gamma_{22}}{4} \right)^2,$$

showing explicitly how non-symmetric dissipation affects the normal-mode dynamics. This expression is the most general form and reduces to simpler structures only after physical symmetry is imposed. Since it was assumed identical ions subjected to the same environment, it is physically reasonable to assume $\gamma_{12} = \gamma_{21}$, and $\gamma_{11} = \gamma_{22} \equiv \gamma$, consistent with the positivity condition $\gamma_{12} \leq \gamma$ obtained in Sec. III. Under these conditions, the eigenvalues simplify to

$$\lambda_{\pm} = \omega_0 \pm \Omega - i \frac{\gamma \pm \gamma_{12}}{2}, \quad (28)$$

which reveal the emergence of collective decay channels. Introducing the symmetric and antisymmetric modes,

$$A = \frac{a_1 + a_2}{\sqrt{2}}, \quad B = \frac{a_1 - a_2}{\sqrt{2}}, \quad (29)$$

the equations of motion become

$$\dot{A}(t) = - \left[i(\omega_0 + \Omega) + \frac{\Gamma_+}{2} \right] A(t) + F_+(t), \quad (30)$$

$$\dot{B}(t) = - \left[i(\omega_0 - \Omega) + \frac{\Gamma_-}{2} \right] B(t) + F_-(t), \quad (31)$$

where the collective decay rates are

$$\Gamma_{\pm} = \gamma \pm \gamma_{12}, \quad (32)$$

and $F_{\pm}(t)$ are effective langevin forces.

Equation (32) demonstrates that the common reservoir induces superradiant and subradiant decay channels. When $\gamma_{12} = 0$ the modes decay at the same rate γ , which is physically equivalent to the case of coupling to two independent local baths. As γ_{12} increases, the symmetric mode A decays faster, while the antisymmetric mode B decays more slowly. At the boundary of complete reservoir correlation, $\gamma_{12} = \gamma$ we obtain

$$\Gamma_+ = 2\gamma, \quad \Gamma_- = 0, \quad (33)$$

and the antisymmetric mode B becomes immune to dissipation—a decoherence-free subspace (DFS). In this regime, all excitations stored in B persist indefinitely, and the system retains a memory of its initial state even in the presence of the thermal reservoir.

Using the general solution (26), and assuming the ions initially not correlated, the mean excitation of ion j takes the compact form

$$\begin{aligned} n_j(t) = & e^{-\gamma t} [n_j(0) \cos^2(\Omega t) + n_l(0) \sin^2(\Omega t)] \\ & + \frac{1}{2} e^{-\gamma t} [n_1(0) + n_2(0)] (\cosh(\gamma_{12} t) - 1) \\ & + \bar{N} [1 - e^{-\gamma t} \cosh(\gamma_{12} t)]. \end{aligned} \quad (34)$$

Figure 1 shows the time dependence of $n_1(t)$ for several values of γ_{12}/γ , assuming the ions are initially in thermal states with mean occupation \bar{n}_1 and \bar{n}_2 . When $\gamma_{12} < \gamma$, both ions relax exponentially to the thermal occupation \bar{N} , whereas if the condition $\gamma_{12} = \gamma$ is satisfied, a fraction of the initial excitations remains trapped indefinitely since

$$n_j(\infty) = \frac{1}{2} \left(\bar{N} + \frac{n_1(0) + n_2(0)}{2} \right). \quad (35)$$

Here $n_j(\infty) \equiv \lim_{t \rightarrow \infty} n_j(t)$, and derivatives are taken before the asymptotic limit. A short-time expansion of Eq. (34), valid for $\gamma t, \gamma_{12} t \ll 1$, further clarifies the influence of correlated dissipation,

$$\begin{aligned} n_j(t) \approx & n_j(0) \cos^2(\Omega t) + n_l(0) \sin^2(\Omega t) + \bar{N} \gamma t \\ & + \frac{1}{2} \left[\frac{\gamma_{12}^2}{2} (n_1(0) + n_2(0)) - \bar{N} (\gamma^2 + \gamma_{12}^2) \right] t^2, \end{aligned} \quad (36)$$

showing that cross-damping modifies the curvature of the short time population dynamics.

These results establish the dynamical regimes relevant for parameter estimation (Sec. V) and for the generation and preservation of entanglement (Sec. VI).

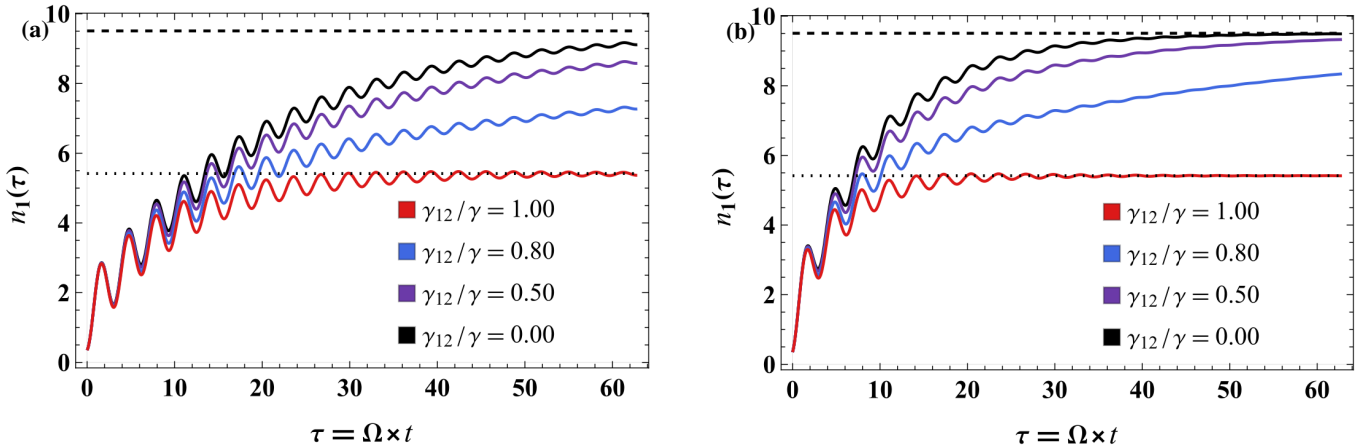


FIG. 1: (Color online) Time evolution of the mean phonon number of ion 1 for several values of the normalized cross-damping rate γ_{12}/γ . The curves, from top to bottom, correspond to $\gamma_{12}/\gamma = 0.00, 0.50, 0.80, 1.00$. The ions are initially prepared in thermal state with $\bar{n}_1 = 0.35$ and $\bar{n}_2 = 2.3$. The black dashed line marks the thermal occupation \bar{N} of the reservoir for $\hbar\omega_0/k_B T = 0.10$, and the black dotted line marks the steady-state population in the fully correlated limit $\gamma_{12} = \gamma$. Panels (a) and (b) correspond to $\gamma/\Omega = 0.05$ and $\gamma/\Omega = 0.10$, respectively. For $\gamma_{12} < \gamma$, both ions relax exponentially to the thermal value \bar{N} . When the critical condition $\gamma_{12} = \gamma$ is reached, a decoherence-free normal mode emerges and part of the initial excitation remains trapped, leading to the modified steady-state value given in Eq. (35).

V. FISHER INFORMATION AND PARAMETER ESTIMATION

The dynamics derived in Sec. IV determine how the motional populations depend on the system parameters and on the degree of reservoir correlation. We now quantify how precisely these parameters can be inferred from energy measurements of a single ion by evaluating the classical Fisher information [14, 15] associated with the parameters θ in the occupation-number distribution $P_1(k; \theta) \equiv P_1(k)$.

Since the system remains Gaussian under linear evolution and Gaussian noise, the reduced state of each ion is fully characterized by the local covariance matrix [16],

$$\mathbf{V}_1(t) = \begin{pmatrix} n_1(t) & m_1(t) \\ m_1^*(t) & n_1(t) \end{pmatrix}, \quad (37)$$

where $n_1(t) = \langle a_1^\dagger(t)a_1(t) \rangle$ and $m_1(t) = -\langle a_1^2(t) \rangle$. The probability of detecting k phonons [3] is then given by

$$P_1(k) = \frac{{}_2F_1\left(\frac{k+1}{2}, \frac{k+2}{2}, 1, z\right)}{\left(1 + \frac{n_1}{n_1^2 - |m_1|^2}\right)^{k+1} \sqrt{n_1^2 - |m_1|^2}}, \quad (38)$$

where ${}_2F_1$ denotes the Gauss hypergeometric function and

$$z = \frac{|m_1|^2}{[n_1(n_1 + 1) - |m_1|^2]^2}. \quad (39)$$

For general initially uncorrelated modes one finds

$$m_1(t) = -\frac{e^{-2i\omega_0 t}}{4} \left[(m_1(0) + m_2(0)) (e^{2i\Omega t} e^{-(\gamma - \gamma_{12})t} + e^{-2i\Omega t} e^{-(\gamma + \gamma_{12})t}) + 2e^{-\gamma t} (m_1(0) - m_2(0)) \right], \quad (40)$$

which depends on the presence of initial fluctuations in at least one of the ions, and vanishes at long times when $\gamma_{12} < \gamma$, while at the decoherence-free condition $\gamma_{12} = \gamma$, it approaches the asymptotic oscillatory form

$$m_1(\infty) = -\frac{m_1(0) + m_2(0)}{4} e^{-2i(\omega_0 + \Omega)t}, \quad (41)$$

with a constant modulus determined by the initial second-order moments.

When both ions start in thermal states, implying zero initial fluctuations ($n_1(0) = n_2(0) = 0$), Eq. (38) simplifies and reduces to the geometric distribution

$$P_1(k) = \frac{n_1(t)^k}{(1 + n_1(t))^{k+1}}, \quad (42)$$

so the full statistics is encoded solely in the mean occupation $n_1(t)$.

The Fisher Information Matrix (FIM) [14, 15] with respect to the parameter vector θ is

$$F_{\alpha\beta} = \sum_k P_1(k; \theta) \frac{\partial \ln P_1(k; \theta)}{\partial \theta_\alpha} \frac{\partial \ln P_1(k; \theta)}{\partial \theta_\beta}, \quad (43)$$

where the diagonal entries are non-negative and measure the sensitivity of the likelihood to individual parameters, with larger values indicating higher precision in estimation. The off-diagonal elements quantify statistical dependencies between parameter estimates – a positive value indicates that increasing parameter θ_α enhances the information available about θ_β , whereas a negative value implies that precise estimation of one parameter reduces the available information about the other.

For the distribution (42), the FIM simplifies to

$$F_{\alpha\beta} = \frac{1}{n_1(t)(1 + n_1(t))} \frac{\partial n_1(t)}{\partial \theta_\alpha} \frac{\partial n_1(t)}{\partial \theta_\beta}, \quad (44)$$

where the parameter vector is

$$\theta = (n_1(0), n_2(0), \Omega, \gamma, \gamma_{12}, \bar{N})^T \equiv (\theta_1, \theta_2, \theta_3, \theta_4, \theta_5, \theta_6)^T, \quad (45)$$

For $0 \leq \gamma_{12} \leq \gamma$ we treat γ and γ_{12} as independent parameters of the dynamical model. Consequently, the Fisher information matrix is computed from Eq. (44) by taking the partial derivatives $\partial_{\theta_\alpha} n_1(t)$ with respect to each component of θ and only afterwards evaluating them at the chosen numerical values of (γ, γ_{12}) . In particular, the decoherence-free condition is incorporated by evaluating the resulting expressions at the point $\gamma_{12} = \gamma$ (rather than imposing $\gamma_{12} = \gamma$ prior to differentiation). This procedure yields a well-defined Fisher matrix and allows a consistent comparison between the fully correlated case and the partially correlated regimes. If one instead assumes an exact constraint $\gamma_{12} = \gamma$ as part of the model definition, then γ_{12} is no longer an independent coordinate and the parameter space must be reduced accordingly. In that constrained description, it is natural to reparametrize the dissipation sector in terms of the collective rates $\Gamma_\pm = \gamma \pm \gamma_{12}$, and in the DFS limit $\Gamma_- = 0$ is fixed while only the remaining independent combination(s) can be estimated from data. In the remainder of this section, however, we keep (γ, γ_{12}) independent and use $\gamma_{12} = \gamma$ only as an evaluation point.

A. Inference of $n_1(0)$, $n_2(0)$, and \bar{N}

Figures 2–4 illustrate three representative elements of the FIM: the diagonal terms F_{11} and F_{66} and the off-diagonal correlation F_{12} . All of them display a pronounced short-time enhancement.

Initially, when coherent evolution dominates,

$$n_1(t) \simeq n_1(0) \cos^2 \Omega t + n_2(0) \sin^2 \Omega t + \mathcal{O}(t), \quad (46)$$

so any parameter that modifies the coherent exchange frequency or the initial energy distribution produces a large curvature in $n_1(t)$ and hence a large FI. This explains the rapid growth of F_{11} and F_{12} during the first few Rabi periods [17], as seen in Figs. 2 and 3. Increasing γ_{12} enhances this effect. Correlated dissipation reduces the effective damping rate of the antisymmetric collective mode B , which becomes subradiant and eventually decoherence free at $\gamma_{12} = \gamma$. This slows down the overall decay of the coherent energy exchange between the ions and increases $\partial_{\theta_\alpha} n_1(t)$ for parameters such as $n_1(0)$, $n_2(0)$, and Ω .

The long-time limit of the FI can be understood from the stationary value of $n_1(t)$,

$$n_1(\infty) = \begin{cases} \bar{N}, & \gamma_{12} < \gamma, \\ \frac{1}{2} \left(\bar{N} + \frac{n_1(0) + n_2(0)}{2} \right), & \gamma_{12} = \gamma. \end{cases} \quad (47)$$

In the case $\gamma_{12} < \gamma$, the steady state is thermal, so

$$\frac{\partial n_1(\infty)}{\partial \theta_\alpha} = 0 \quad \text{for all } \theta_\alpha \neq \bar{N}. \quad (48)$$

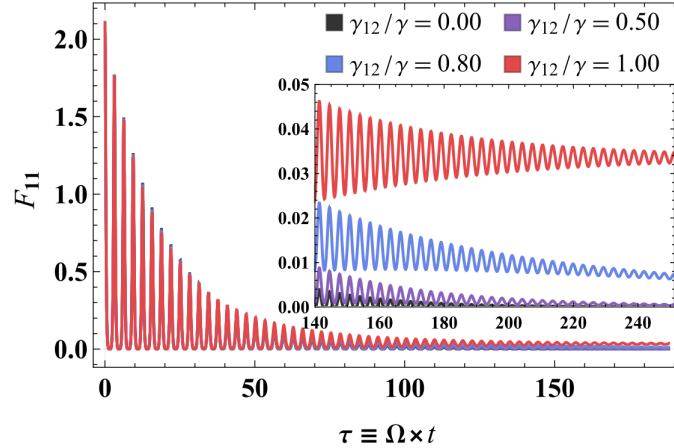


FIG. 2: (Color online) Fisher information element F_{11} , quantifying the sensitivity of the phonon-number distribution to the initial occupation $n_1(0)$, for several values of the normalized cross-damping rate γ_{12}/γ with the initial conditions $\bar{n}_1 = 0.35$, $\bar{n}_2 = 2.3$, $\hbar\omega_0/k_B T = 1.0$, $\gamma/\Omega = 0.02$ and $\Omega = 3.1\pi\text{kHz}$. The curves, from bottom to top, correspond to $\gamma_{12}/\gamma = 0.00, 0.50, 0.80, 1.00$. For weakly correlated dissipation, F_{11} displays damped Rabi oscillations whose envelope decays at rate γ . As γ_{12} increases, the decay slows down and the short-time peak broadens. When the fully correlated condition $\gamma_{12} = \gamma$ is reached, a decoherence-free subspace forms and F_{11} saturates to a nonzero long-time plateau, indicating persistent information about the initial state. The inset shows the long-time behavior toward the respective steady-state values

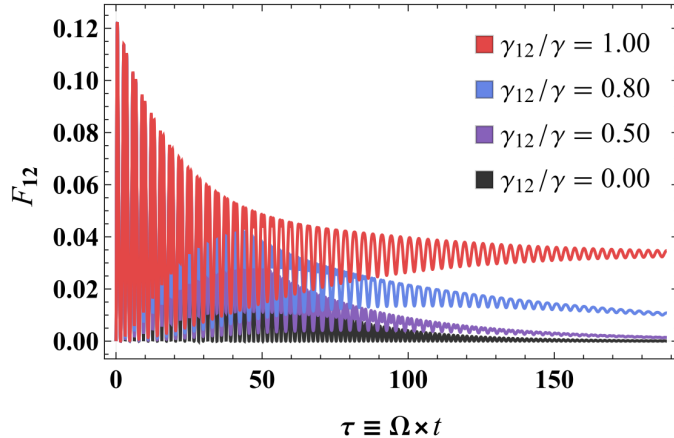


FIG. 3: (Color online) Fisher information element F_{12} , describing correlations between the estimators of the initial occupations $n_1(0)$ and $n_2(0)$ for several values of the normalized cross-damping rate γ_{12}/γ with the initial conditions $\bar{n}_1 = 0.35$, $\bar{n}_2 = 2.3$, $\hbar\omega_0/k_B T = 1.0$, $\gamma/\Omega = 0.02$ and $\Omega = 3.1\pi\text{kHz}$. The curves, from bottom to top, correspond to $\gamma_{12}/\gamma = 0.00, 0.50, 0.80, 1.00$. For $\gamma_{12} = 0$, F_{12} oscillates around zero as excitations are periodically exchanged between ions through the coherent coupling Ω . Increasing γ_{12} leads to an asymmetric oscillation pattern and an overall enhancement of short-time sensitivity. In the fully correlated case $\gamma_{12} = \gamma$, a nonzero long-time plateau emerges due to the decoherence-free subspace, indicating that correlations between the initial occupations remain encoded in the asymptotic state.

Hence, by Eq. (44),

$$F_{\alpha\beta}(t \rightarrow \infty) = 0, \quad (\alpha, \beta) \neq (\bar{N}, \bar{N}). \quad (49)$$

This behavior appears clearly in Fig. 4 the FI associated with the reservoir occupation \bar{N} saturates to a finite asymptotic value, whereas F_{11} and F_{12} decay to zero when $\gamma_{12} < \gamma$.

In the fully correlated case $\gamma_{12} = \gamma$, a decoherence-free subspace (DFS) is formed, and

$$\frac{\partial n_1(\infty)}{\partial \theta_\alpha} \neq 0 \quad \text{for all } \theta_\alpha \neq \Omega, \quad (50)$$

so part of the initial population remains indefinitely encoded in $n_1(t)$. Thus, F_{11} and F_{12} acquire a nonzero long-time plateau

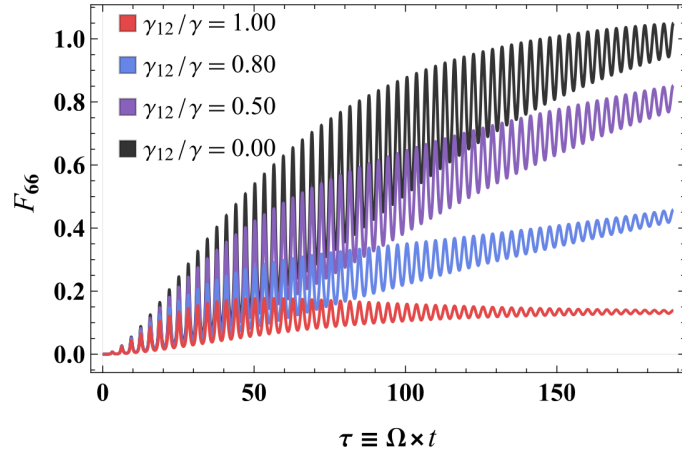


FIG. 4: (Color online) Fisher information element F_{66} associated with the estimability of the reservoir thermal occupation \bar{N} for several values of the normalized cross-damping rate γ_{12}/γ with the initial conditions $\bar{n}_1 = 0.35$, $\bar{n}_2 = 2.3$, $\hbar\omega_0/k_B T = 1.0$, $\gamma/\Omega = 0.02$ and $\Omega = 3.1\pi\text{kHz}$. The curves, from top to bottom, correspond to $\gamma_{12}/\gamma = 0.00, 0.50, 0.80, 1.00$. For all values of the correlation parameter γ_{12}/γ , F_{66} monotonically increases at short times and saturates to a finite constant. This reflects that the steady-state phonon number always carries information about the reservoir temperature, whereas the influence of correlated dissipation affects only the transient dynamics. Unlike the FI elements associated with initial occupations, F_{66} does not vanish at long times even when the bath is uncorrelated.

[see Figs. 2 and 3]. In contrast, F_{66} retains its usual thermal asymptote, since the steady-state temperature is unaffected by the DFS.

The specific features relevant for inference can now be summarized. The element F_{11} , shown in Fig. 2, quantifies the sensitivity to the initial occupation $n_1(0)$. For small γ_{12} it displays damped oscillations with an envelope decaying at the single-ion rate γ . As γ_{12} increases, the decay of the envelope slows down, and when $\gamma_{12} = \gamma$ a clear nonzero plateau emerges at long times. This persistent FI is a direct signature of the DFS and indicates that measurements performed at arbitrarily late times retain information about the initial state. By symmetry, an analogous behavior would be obtained for F_{22} , associated with $n_2(0)$.

The element F_{66} , displayed in Fig. 4, describes the sensitivity to the reservoir occupation \bar{N} . Unlike the FI for initial-state parameters, F_{66} envelope grows monotonically at short times and saturates to a finite constant for all values of γ_{12} . Correlated dissipation modifies the transient dynamics, but the asymptotic FI is almost independent of γ_{12} , reflecting the fact that the steady state is always thermal and that the temperature parameter remains fully estimable.

While the diagonal FIM elements are relevant for single-parameter estimation, the off-diagonal ones are crucial for joint inference. This is exemplified by F_{12} , which represents the correlation between the estimators of $n_1(0)$ and $n_2(0)$, as shown in Fig. 3. For $\gamma_{12} = 0$, F_{12} oscillates around zero because excitations periodically exchange between the two ions. As γ_{12} increases, the oscillations become less symmetric, and a nonzero asymptotic value appears when $\gamma_{12} = \gamma$. This plateau indicates that the DFS not only preserves information about each initial occupation but also about their correlation, viewed as parameters of the estimation problem.

B. Estimation of trap and dissipation parameters: Ω , γ , and γ_{12}

In addition to initial-state parameters and the reservoir occupation, the Fisher information also quantifies the estimability of the intrinsic trap and dissipation parameters – the coherent coupling Ω (controlled by the inter-ion Coulomb repulsion), the local damping rate γ , and the cross-damping rate γ_{12} . These appear respectively in the FIM elements F_{33} , F_{44} , and F_{55} .

Figures 5–7 show the behavior of these FIM elements for representative values of γ_{12}/γ . Their structure reflects the fact that Ω , γ , and γ_{12} influence the dynamics only through transient behavior, since none of these parameters appear explicitly in the long-time steady state (except indirectly when the DFS is formed). We now discuss the inference of the three separate parameters.

Figure 5 shows that the Fisher information F_{33} associated with the coherent coupling Ω shows the transient coherent oscillations in the population dynamics. Increasing the cross-damping γ_{12} does not show a significant change in the profile of F_{33} , keeping the finite-time sensitivity to Ω qualitatively the same in all instances of the rate γ_{12}/γ . Since the steady-state population is independent of Ω , F_{33} vanishes asymptotically for all values of γ_{12} , including at the decoherence-free point $\gamma_{12} = \gamma$, making the estimation of Ω intrinsically a finite-time task.

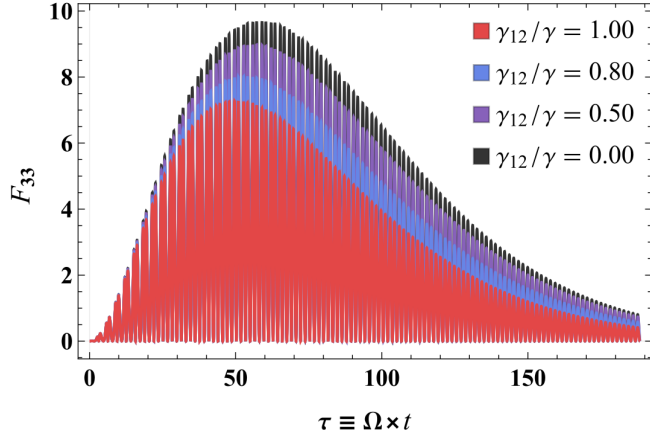


FIG. 5: (Color online) Fisher information element F_{33} associated with estimating the coherent coupling Ω for several values of the normalized cross-damping rate γ_{12}/γ with the initial conditions $\bar{n}_1 = 0.35$, $\bar{n}_2 = 2.3$, $\hbar\omega_0/k_B T = 1.0$, $\gamma/\Omega = 0.02$ and $\Omega = 3.1\pi\text{kHz}$. The curves, from top to bottom, correspond to $\gamma_{12}/\gamma = 0.00, 0.50, 0.80, 1.00$. The FI displays oscillations at short and intermediate times, reflecting the sensitivity of $n_1(t)$ to the coherent exchange of excitations. Increasing the cross-damping γ_{12} slows the decay of the envelope and enhances the time window over which Ω can be accurately inferred. For $\gamma_{12} < \gamma$, F_{33} vanishes at long times since the steady state does not retain information about the coherent coupling.

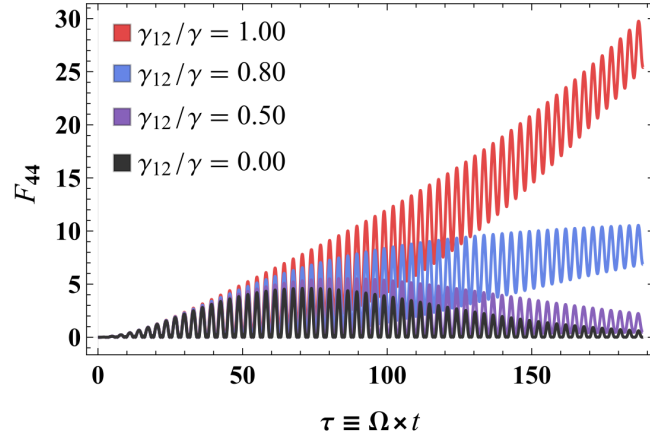


FIG. 6: (Color online) Fisher information element F_{44} related to the estimation of the local damping rate γ for several values of the normalized cross-damping rate γ_{12}/γ with the initial conditions $\bar{n}_1 = 0.35$, $\bar{n}_2 = 2.3$, $\hbar\omega_0/k_B T = 1.0$, $\gamma/\Omega = 0.02$ and $\Omega = 3.1\pi\text{kHz}$. The curves, from bottom to top, correspond to $\gamma_{12}/\gamma = 0.00, 0.50, 0.80, 1.00$. The FI peaks around times of order γ^{-1} , where the dissipative contribution to the dynamics dominates over coherent exchange. Correlated dissipation broadens this peak and enhances short-time sensitivity. In all cases with $\gamma_{12} < \gamma$, the FI vanishes at long times because the steady-state population carries no information about γ .

The FIM element F_{44} , shown in Fig. 6, characterizes the ability to infer the local damping rate of each ion. Since γ governs the rate at which excitations leak into the reservoir, F_{44} peaks when the dissipative contribution dominates over coherent exchange, typically at times comparable to γ^{-1} . As γ_{12} increases, the interplay between Γ_+ and Γ_- modifies the decay envelope, broadening the region of high sensitivity. Nevertheless, because γ affects only the transient dynamics, $F_{44}(t \rightarrow \infty) = 0$ for all $\gamma_{12} < \gamma$. We shall talk about the behavior of F_{44} in the regime $\gamma_{12} = \gamma$ latter on.

In Figure 7 F_{55} displays the FIM element associated with the cross-damping. Compared with F_{33} and F_{44} , the FI for γ_{12} exhibits the strongest dependence on reservoir correlations. When γ_{12} is small, the effect of cross-damping is weak and the corresponding FI remains small. As γ_{12} increases, the FI grows rapidly – the curvature of $n_1(t)$ with respect to γ_{12} becomes larger because this parameter directly controls the splitting of the collective decay rates Γ_{\pm} . Near the boundary $\gamma_{12} \rightarrow \gamma$, similar to F_{44} , the FI develops a tall and broad peak, indicating that cross-damped dynamics can be extremely sensitive to small changes in γ_{12} . As for F_{44} , at $\gamma_{12} = \gamma$ the curve shows an envelope increasing with t^2 .

The off-diagonal Fisher information element F_{45} (shown in Fig. (8)) quantifies the statistical correlation between the estimators of the local damping rate γ and the cross-damping rate γ_{12} . Since both parameters enter the dynamics through the collective

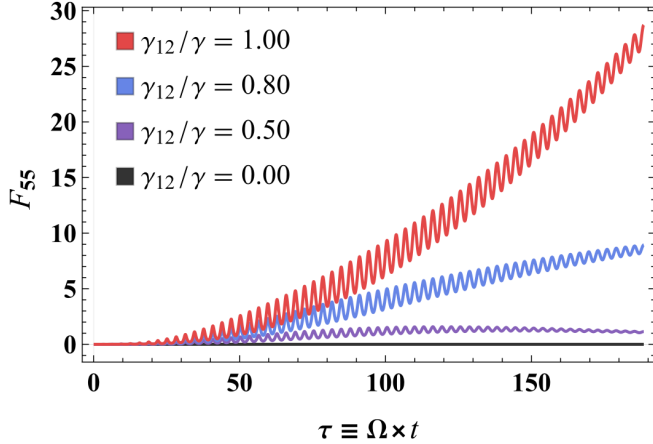


FIG. 7: (Color online) Fisher information element F_{55} corresponding to the estimation of the cross-damping rate γ_{12} for several values of the normalized cross-damping rate γ_{12}/γ with the initial conditions $\bar{n}_1 = 0.35$, $\bar{n}_2 = 2.3$, $\hbar\omega_0/k_B T = 1.0$, $\gamma/\Omega = 0.02$ and $\Omega = 3.1\pi\text{kHz}$. The curves, from bottom to top, correspond to $\gamma_{12}/\gamma = 0.00, 0.50, 0.80, 1.00$. The FI exhibits a strong dependence on γ_{12} : for weak cross-damping the sensitivity is low, but it increases rapidly as γ_{12} approaches γ . Near the fully correlated regime, the FI develops a broad and pronounced peak, reflecting the strong influence of γ_{12} on the collective decay rates. As with other transient parameters, F_{55} decays to zero at long times unless the decoherence-free condition is satisfied.

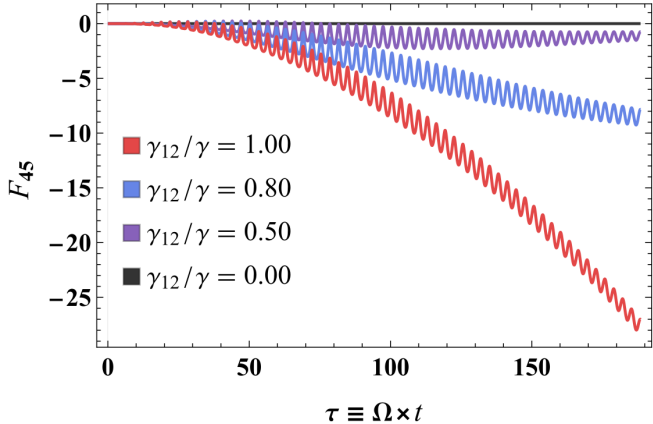


FIG. 8: (Color online) Fisher information element F_{45} corresponding to the simultaneous estimation of the local, γ , and cross-damping for several values of the normalized cross-damping rate γ_{12}/γ with the initial conditions $\bar{n}_1 = 0.35$, $\bar{n}_2 = 2.3$, $\hbar\omega_0/k_B T = 1.0$, $\gamma/\Omega = 0.02$ and $\Omega = 3.1\pi\text{kHz}$. The curves, from top to bottom, correspond to $\gamma_{12}/\gamma = 0.00, 0.50, 0.80, 1.00$ rates.

decay rates $\Gamma_{\pm} = \gamma \pm \gamma_{12}$, F_{45} is generally negative, indicating an anticorrelation between their estimates. As γ_{12} increases, this anticorrelation becomes stronger, reflecting the growing sensitivity of the dynamics to the balance between local and collective dissipation. Near the fully correlated regime $\gamma_{12} \rightarrow \gamma$, F_{45} acquires a large magnitude and a broad temporal profile, signaling that the dynamics constrain primarily the difference $\gamma - \gamma_{12}$ rather than the individual rates.

This is essential for understanding the behavior of F_{44} , and F_{55} , and, at the fully correlated limit $\gamma_{12} = \gamma$. In this regime $\gamma_{12} = \gamma$ the curve envelope of the curve for F_{44} , F_{55} monotonically increases with t^2 , since by taking the derivatives of (34) in respect to γ_{12} , or γ and taking the limit of $t \rightarrow \infty$, leads to

$$\frac{\partial n_1(\infty)}{\partial \gamma} \sim -\frac{\partial n_1(\infty)}{\partial \gamma_{12}} \sim \frac{t}{2} \left[\bar{N} - \frac{(n_1(0) + n_2(0))}{2} \right]. \quad (51)$$

Although the steady-state population in Eq. (47) does not depend on γ or γ_{12} individually, the observed scaling $F_{44} = F_{55} = -F_{45} \propto t^2$ at long times indicates that the system nevertheless develops enhanced sensitivity to the equality $\gamma_{12} = \gamma$.

This apparent paradox is resolved by recognizing that while individual estimates of γ and γ_{12} would indeed have zero Fisher Information at infinite time, their difference $\Gamma_- = \gamma - \gamma_{12}$ becomes increasingly estimable. The quadratic growth in F_{44} and

F_{55} reflects the system's growing ability to detect deviations from the DFS condition $\Gamma_- = 0$, even though the absolute values of γ and γ_{12} remain inaccessible. Physically, this means that at long times, the system acts as an increasingly precise null detector that cannot determine what the damping rates are, but it can determine with improving accuracy whether they are equal. The equality $F_{44} = F_{55}$ and perfect anti-correlation in F_{45} , for large times, indicate that any change in γ is indistinguishable from an opposite change in γ_{12} , only their difference matters for the dynamics.

This behavior illustrates a fundamental feature of estimation at parameter boundaries. FI can grow indefinitely for certain parameter combinations while decaying to zero for others. In our case, the combination $\Gamma_- = \gamma - \gamma_{12}$ acquires a Fisher Information that scales as t^2 at long times, allowing the equality condition $\gamma_{12} = \gamma$ to be verified with variance decreasing as $1/t^2$. Meanwhile, information about the sum $\Gamma_+ = \gamma + \gamma_{12}$ is lost in the long-time limit, reflecting that only the difference Γ_- determines whether a DFS exists, while the absolute damping rates become irrelevant for the asymptotic state.

C. Cramér–Rao bound and attainable precisions

The Fisher information matrix $F_{\alpha\beta}(t)$ sets a fundamental lower bound on the covariance matrix of any unbiased estimators $\hat{\theta}$ constructed from the phonon-number statistics $P_1(k; \theta)$. For a sufficiently large number M of independent repetitions of the energy measurement, the (classical) Cramér–Rao bound reads

$$\text{Cov}[\hat{\theta}] \geq \frac{1}{M} \mathbf{F}^{-1}(t), \quad (52)$$

where the inequality is understood in the sense of positive semidefinite matrices. Throughout our analysis, the parameters γ and γ_{12} are treated as independent quantities, so that the Fisher information matrix and the associated Cramér–Rao bounds remain defined even at the decoherence-free point $\gamma_{12} = \gamma$.

For single-parameter estimation (or when the remaining parameters are known), the variance of an unbiased estimator $\hat{\theta}_\alpha$ satisfies

$$\text{Var}(\hat{\theta}_\alpha) \geq \frac{1}{M F_{\alpha\alpha}(t)}. \quad (53)$$

Equations (52) and (53) provide a direct metrological interpretation of the Fisher-information dynamics shown in Figs. 2–4. The short-time enhancement of F_{11} and F_{12} implies that, for fixed M , the minimal achievable uncertainties in the initial occupations $n_1(0)$ and $n_2(0)$ are reduced as the cross-damping γ_{12} increases, with the largest gain occurring near the fully correlated regime. Similarly, the long-time saturation of F_{66} shows that the reservoir temperature (or thermal occupation \bar{N}) remains estimable even after all other parameters have become inaccessible. In the decoherence-free regime $\gamma_{12} = \gamma$, the nonvanishing asymptotic values of F_{11} and F_{12} translate into strictly positive lower bounds for the precision of estimating the initial occupations from arbitrarily late measurements, a feature absent for independent baths.

The same Cramér–Rao analysis also clarifies the attainable precision for estimating the intrinsic trap and dissipation parameters, namely the coherent coupling Ω , the local damping rate γ , and the cross-damping rate γ_{12} , associated with the FI elements F_{33} , F_{44} , F_{55} , respectively (see Figs. 5–7). In all three cases, the corresponding Fisher information exhibits pronounced peaks at short and intermediate times, reflecting the fact that these parameters influence the dynamics only through transient behavior. Consequently, the Cramér–Rao bound indicates that Ω , γ , and γ_{12} must be inferred from measurements performed before the system reaches its steady state. Correlated dissipation enhances these transient FI peaks by slowing the decay of collective modes, thereby widening the temporal window over which accurate estimation of these parameters is possible. However, since none of these parameters appear explicitly in the generic long-time steady state, the corresponding FI elements vanish asymptotically for $\gamma_{12} < \gamma$, and their estimation cannot rely on late-time data. For $\gamma_{12} = \gamma$ the asymptotic t^2 scaling of F_{44} , F_{55} , and F_{45} suggests that trapped ion systems near collective dissipation regimes can serve as sensitive probes for verifying decoherence-free conditions, with precision that improves linearly with measurement time, despite their inability to determine individual damping rates.

The results above can be directly mapped onto an experimentally feasible protocol for parameter inference in trapped-ion platforms. A typical sequence proceeds as follows: (i). Prepare the ions in initial thermal states with controlled occupations $n_1(0)$ and $n_2(0)$ (or in squeezed-thermal states for entanglement studies, as discussed in Sec. VI). (ii). Allow the ions to evolve for a chosen interrogation time t , during which the combined action of coherent coupling Ω , local damping γ , and cross-damping γ_{12} shapes the motional populations. (iii). Perform phonon-number-resolved fluorescence detection on ion 1, yielding a sample $\{k_1, k_2, \dots, k_M\}$ drawn from the distribution $P_1(k; t)$ in Eq. (42). (iv). Construct unbiased estimators $\hat{\theta}_\alpha$ for the parameters of interest, with attainable precision bounded by the Cramér–Rao inequality (53).

The time dependence of the Fisher information determines the optimal measurement strategy. Early-time measurements are optimal for estimating Ω , γ , γ_{12} , $n_1(0)$, and $n_2(0)$, whereas late-time measurements provide maximal sensitivity to the reservoir occupation \bar{N} . In the decoherence-free regime $\gamma_{12} = \gamma$, long-time measurements also retain finite information about the initial occupations, offering enhanced robustness against decoherence.

Finally, three qualitatively distinct estimation regimes can be identified. For independent baths ($\gamma_{12} = 0$), local damping causes all FI elements except F_{66} to vanish at long times, so that only the bath temperature remains asymptotically estimable. For partially correlated baths ($0 < \gamma_{12} < \gamma$), the FI is substantially enhanced at short times—particularly for the initial-state and trap parameters—but all information about these quantities is eventually lost as the system relaxes to a thermal steady state. In the fully correlated case ($\gamma_{12} = \gamma$), a decoherence-free subspace is formed with the long-time FI associated with $n_1(0)$, $n_2(0)$, and their correlations remains finite due to incomplete relaxation of the antisymmetric mode, whereas the FI for parameters that enter only through transient dynamics, such as Ω , γ , and γ_{12} itself, still decays to zero and must be accessed through short-time measurements. Correlated dissipation therefore not only enhances parameter sensitivity in the transient regime but can also preserve information about selected parameters indefinitely, defining clear operating conditions under which dissipative trapped-ion systems function as robust probes of both system and reservoir properties.

Remark that we have focused on the classical Fisher information associated with phonon-number measurements, which constitute a natural and experimentally accessible observable in trapped-ion systems. The corresponding quantum Fisher information (QFI), which quantifies the ultimate precision attainable with optimal measurements, generally exceeds or equals the classical FI considered here. A full QFI analysis would require diagonalizing the Gaussian states generated by the cross-damped dynamics and optimizing over all physically allowed POVMs, which is beyond the scope of the present investigation. Nevertheless, the classical FI already captures the key qualitative features: the enhancement of short-time sensitivity with increasing reservoir correlation, the privileged estimability of \bar{N} at long times, and the preservation of initial-state information in the decoherence-free regime.

VI. ENTANGLEMENT GENERATION AND PRESERVATION

Correlated dissipation also has important consequences for the development and robustness of nonclassical correlations between the motional modes. In this section we analyze how the cross-damping rate γ_{12} affects the creation, protection, and lifetime of Gaussian entanglement, focusing on initially thermal-squeezed product states and applying the PPT criterion for Gaussian states [18, 19]. The Gaussian-state framework and non-classicality criteria employed here build on previous analyses of trapped-ion motional dynamics in the absence of dissipation, where squeezing was identified as a key non-classical resource [13].

Because the global state remains Gaussian for all times, its entanglement properties are fully determined by the covariance matrix

$$\mathbf{V}(t) = \begin{pmatrix} \mathbf{V}_1(t) & \mathbf{C}(t) \\ \mathbf{C}^\dagger(t) & \mathbf{V}_2(t) \end{pmatrix}. \quad (54)$$

The Peres–Horodecki PPT criterion reduces to a positivity condition for the partially transposed covariance matrix. Following Refs. [16, 18, 19], we quantify entanglement via the symplectic invariant

$$Y(t) = I_1 I_2 + \left(\frac{1}{4} - |I_3| \right)^2 - I_4 - \frac{1}{4}(I_1 + I_2), \quad (55)$$

where $I_1 = \det \mathbf{V}_1$, $I_2 = \det \mathbf{V}_2$, $I_3 = \det \mathbf{C}$, and I_4 is a fourth-order invariant. The condition $Y(t) < 0$ is a necessary and sufficient condition to the presence of entanglement for Gaussian states. P-representable (Classical) states on each initial vibrational mode will not get entangled due to the nature of the direct interaction or the indirect interaction via the common thermal reservoir [18, 20]. Therefore, we consider ion 1 initially in a thermal state with $n_1(0) = \bar{n}_1$, $m_1(0) = 0$ and ion 2 in a squeezed thermal state with squeezing parameter r and phase $\theta = 0$, so that $n_2(0) = (\bar{n}_2 + 1/2) \cosh(2r) - 1/2$, and $m_2(0) = (\bar{n}_2 + 1/2) \sinh(2r)$. This choice allows us to study how initial squeezing influences entanglement generation under correlated dissipation. Since $\mathbf{C}(0) = 0$, any entanglement must be generated dynamically—either by the coherent coupling Ω or by the correlated reservoir. Now, a thermal squeezed state can be non-classical, depending on the balance between r and the initial thermal population of mode 2, and the direct or indirect (via reservoir) interaction will be able to entangle the ions vibrational modes.

Figure 9(a) summarizes the case of uncoupled ions ($\Omega = 0$), where the common reservoir is the only mechanism capable of creating correlations. The upper 3D surface in Fig. 9(a) shows the region in the parameter space $(\tau, \gamma_{12}/\gamma, \hbar\omega_0/k_B T)$ for which $Y(\tau) < 0$. Entanglement appears only when the cross-damping is sufficiently strong. In particular, as γ_{12}/γ approaches unity, a transient domain with $Y < 0$ opens up and widens, revealing genuinely reservoir-induced entanglement. This entanglement is very sensitive to temperature. Larger values of $\hbar\omega_0/k_B T$ (lower thermal occupation) enlarge the negative- Y region, whereas higher temperatures quickly suppress it.

The lower panel of Fig. 9(a) shows the corresponding time dependence of $Y(\tau)$ for a fixed squeezing parameter. At very early times, $Y > 0$ because the ions are still essentially uncorrelated. As the common dissipation builds up correlations, $Y(\tau)$ becomes negative over a finite time window. At longer times, local heating dominates and Y returns to positive values. For $\gamma_{12}/\gamma \simeq 1$,

this negative window is substantially extended, showing that strongly correlated reservoirs not only generate entanglement but also delay its degradation even in the absence of any coherent coupling.

When the ions are coupled through the exchange Hamiltonian ($\Omega \neq 0$), the entanglement dynamics change qualitatively. Figure 9(b) displays density plots of $Y(\tau)$ as a function of time and squeezing r for several values of γ_{12}/γ , corresponding to the four panels shown. For $\gamma_{12} = 0$ [upper-left panel of Fig. 9(b)], entanglement is generated at early times due to the beam-splitter mixing of the squeezed mode into the thermal one. The blue regions ($Y < 0$) indicate intervals during which the coherent transfer of squeezing leads to a bipartite nonclassical state. As γ_{12} increases to intermediate values [upper-right and lower-left panels of Fig. 9(b)], two trends become apparent: the first entanglement window becomes broader, and the subsequent revivals decay more slowly. This behavior reflects the fact that reservoir correlations modify the collective decay rates of the normal modes, partially protecting the nonclassical fluctuations stored in them. In the fully correlated case $\gamma_{12} = \gamma$ [lower-right panel of Fig. 9(b)], the entanglement windows persist for significantly longer times. Here the antisymmetric normal mode B becomes decoherence free and retains a finite fraction of the initial squeezing indefinitely. The correlated reservoir thus plays a protective role; it reduces the effective damping of the entangled mode and slows the loss of quantum correlations, even though the local motional states of the ions continue to thermalize.

The comparison between Fig. 9(a) and Fig. 9(b) highlights the different roles played by coherent coupling and correlated dissipation. For uncoupled ions ($\Omega = 0$), entanglement is generated purely by the common reservoir, requires strong cross-damping, and survives only within a transient time window before thermal noise dominates. For coupled ions ($\Omega \neq 0$), entanglement is created mainly by coherent squeezing transfer, while the correlated reservoir acts as a stabilizing mechanism that enhances the size and duration of the entangled regions. In the fully correlated regime $\gamma_{12} = \gamma$, the emergence of a decoherence-free subspace provides the strongest enhancement and leads to long-lived entanglement. These results confirm that cross-correlated reservoirs can be exploited as a resource for engineering and protecting nonclassical motional states in trapped-ion systems.

Remark that although our separability analysis relies on the sign of the invariant $Y(\tau)$ to detect entanglement, its amount is also reflected in the Minkowski structure of Y , as established in Ref. [21]. In that formulation, the negativity of Y is not only a binary indicator of nonseparability but also quantifies, through its depth, the distance of the state from the boundary of the separable set in the associated pseudo-Riemannian geometry. Thus, the separability surfaces shown in Fig. 9 capture not only the onset of entanglement but also, through the magnitude of Y , the geometric robustness of the generated quantum correlations in the sense of the Minkowski metric structure of Gaussian-state entanglement.

VII. CONCLUSIONS

We have investigated the dynamics of two trapped ions interacting with a common thermal reservoir, focusing on how cross-correlated dissipation modifies heating, relaxation, parameter sensitivity, and entanglement generation. Starting from a microscopic system-reservoir model, we derived the corresponding Heisenberg-Langevin equations and identified the emergence of collective decay channels with rates $\Gamma_{\pm} = \gamma \pm \gamma_{12}$. When the cross-damping reaches its maximal value $\gamma_{12} = \gamma$, the antisymmetric normal mode becomes decoherence free, allowing a fraction of the initial motional population to persist indefinitely. The altered decay structure has direct implications for metrology. Using the Fisher information associated with phonon-number measurements, we showed that reservoir correlations enhance short-time sensitivity to both system and bath parameters by slowing the decay of coherent energy exchange. For $\gamma_{12} < \gamma$, all information except that associated with the reservoir temperature is lost at long times, whereas in the fully correlated regime the decoherence-free subspace preserves a finite amount of information about the initial motional populations. Thus, correlated dissipation can improve transient estimation accuracy and, in special regimes, prevent the complete asymptotic loss of selected parameters. The entanglement analysis further illustrates the role of the common reservoir. For uncoupled ions, cross-damping alone can generate entanglement, though only under strong reservoir correlations and sufficiently low temperatures. When coherent coupling is present, reservoir correlations protect part of the nonclassical fluctuations exchanged between the ions, extending entanglement lifetimes; at $\gamma_{12} = \gamma$, the decoherence-free mode yields particularly long-lived entanglement windows.

The parameter regimes explored in this work are compatible with current trapped-ion experiments. Typical axial trap frequencies in the range $\omega_0/2\pi \sim 0.1\text{--}2$ MHz, coherent coupling strengths $\Omega/2\pi$ of a few kHz, and heating rates $\gamma/2\pi$ from a few Hz to tens of Hz are routinely reported. Correlated dissipation naturally arises from shared electrodes, common voltage sources, and finite correlation lengths of surface electric-field noise, and can be further engineered using controlled noise injection or tailored reservoir engineering schemes. In this context, the Fisher-information analysis presented here provides direct guidance for optimal interrogation times and parameter regimes: transient measurements maximize sensitivity to Ω , γ , and γ_{12} , while late-time measurements allow verification of decoherence-free conditions through the enhanced sensitivity to the difference $\Gamma_- = \gamma - \gamma_{12}$. These features suggest that correlated dissipation can be exploited not only as a source of noise, but also as a diagnostic and metrological resource for characterizing dissipation mechanisms and verifying collective decoherence suppression in trapped-ion platforms. The framework developed here provides practical guidance for exploiting common-reservoir effects in trapped-ion systems and identifies operating regimes in which dissipation can serve as a controlled resource for precision sensing, reservoir engineering, and quantum-state manipulation.

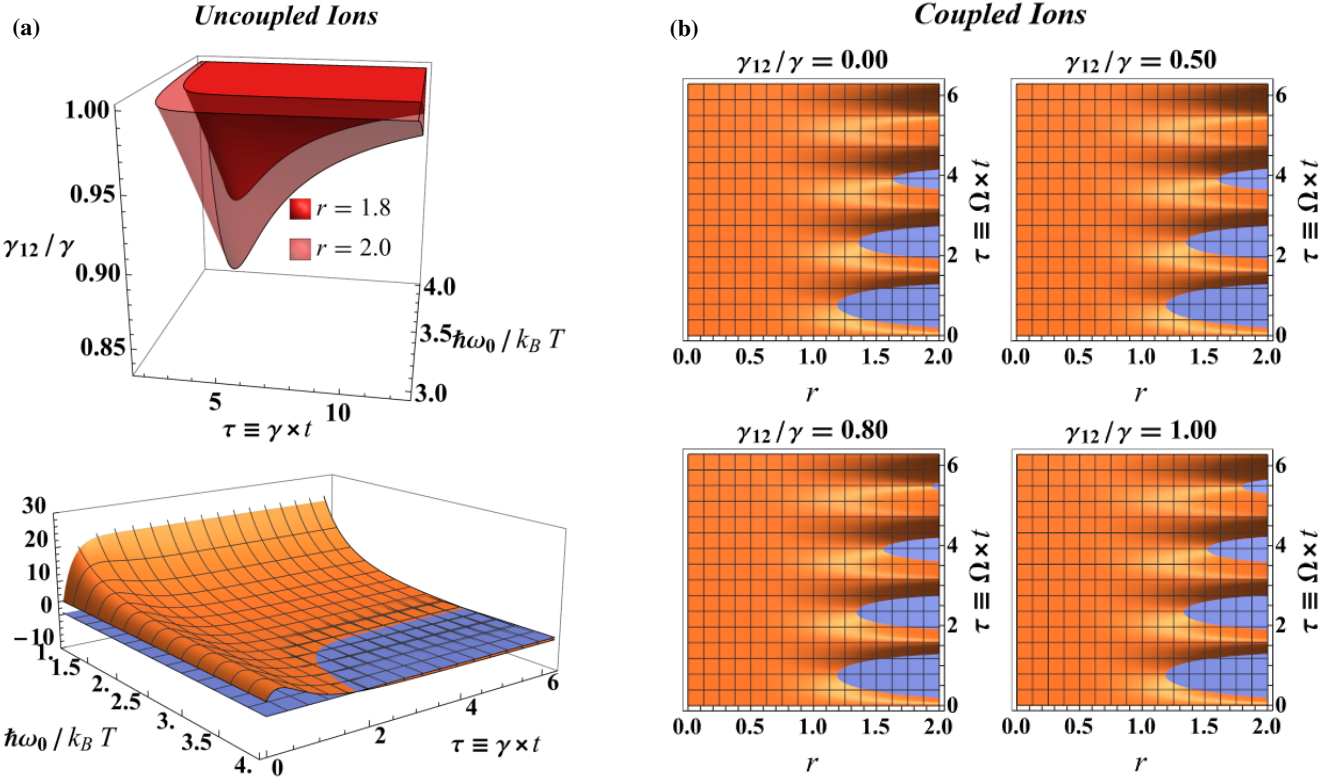


FIG. 9: Separability function $Y(\tau)$ for Gaussian states of the two motional modes. (a) Parameter region for reservoir-induced entanglement in the absence of coherent coupling ($\Omega = 0$). The upper 3D surface shows the domain in the space $(\tau, \gamma_{12}/\gamma, \hbar\omega_0/k_B T)$ where $Y(\tau) < 0$, while the lower panel displays the time dependence of $Y(\tau)$ for a fixed squeezing parameter $r = 2.0$ and $\gamma_{12} = \gamma$, with negative values signaling entanglement. (b) Entanglement dynamics for coherently coupled ions ($\Omega \neq 0$), shown as density plots of $Y(\tau)$ as a function of time and squeezing r for several values of the normalized cross-damping γ_{12}/γ (increasing from the upper-left to the lower-right panel of the composite image). Blue (negative) regions correspond to entangled states, illustrating how increasing reservoir correlations enlarge and prolong the time windows where $Y(\tau) < 0$, with the longest-lived entanglement obtained near the fully correlated regime $\gamma_{12} = \gamma$.

ACKNOWLEDGMENTS

CFPA acknowledge the support from the Coordenação de Aperfeiçoamento de Pessoal de Nível Superior – Brasil (CAPES) – Finance Code 001. MCO acknowledges partial financial support from the National Institute of Science and Technology for Applied Quantum Computing through CNPq process No. 408884/2024-0 and by FAPESP, through the Center for Research and Innovation on Smart and Quantum Materials (CRISQuaM) process No. 2013/07276-1.

[1] K. R. Brown, C. Ospelkaus, Y. Colombe, A. C. Wilson, D. Leibfried, and D. J. Wineland, Coupled quantized mechanical oscillators, *Nature* **471**, 196 (2011).

[2] M. Harlander, R. Lechner, M. Brownnutt, R. Blatt, and W. Hänsel, Trapped-ion antennae for the transmission of quantum information, *Nature* **471**, 200 (2011).

[3] O. de Sá Neto, H. Costa, G. Prataviera, and M. C. de Oliveira, Temperature estimation of a pair of trapped ions, *Sci. Rep.* **12**, 6697 (2022).

[4] L. Mandel and E. Wolf, *Optical Coherence and Quantum Optics* (Cambridge University Press, 1995).

[5] D. Braun, Creation of entanglement by interaction with a common heat bath, *Phys. Rev. Lett.* **89**, 277901 (2002).

[6] F. Benatti, R. Floreanini, and M. Piani, Environment induced entanglement in markovian dissipative dynamics, *Phys. Rev. Lett.* **91**, 070402 (2003).

[7] J. P. Paz and A. J. Roncaglia, Dynamics of the entanglement between two oscillators in the same environment, *Phys. Rev. Lett.* **100**, 220401 (2008).

[8] A. Romanelli, A. Vallejo, A. Auyuanet, and R. Donangelo, Critical temperature for the existence of entanglement in the bell-diagonal states, *Phys. Lett. A* **451**, 128426 (2022).

- [9] J.-H. An, S.-J. Wang, and H.-G. Luo, Entanglement dynamics of qubits in a common environment, *Physica A* **382**, 753 (2007).
- [10] A. Wolf, G. De Chiara, E. Kajari, E. Lutz, and G. Morigi, Entangling two distant oscillators with a quantum reservoir, *EPL* **95**, 60008 (2011).
- [11] J. S. Prauzner-Bechcicki, Two-mode squeezed vacuum state coupled to the common thermal reservoir, *J. Phys. A* **37**, L173 (2004).
- [12] A. De Castro, R. Siqueira, and V. Dodonov, Effect of dissipation and reservoir temperature on squeezing exchange and emergent entanglement in two coupled bosonic modes, *Phys. Lett. A* **372**, 367 (2008).
- [13] C. F. P. Avalos and M. C. de Oliveira, Non-classicality and non-adiabaticity in a single trapped ion, *New Journal of Physics* **27**, 023028 (2025).
- [14] B. R. Frieden, *Science from Fisher Information* (Cambridge University Press, Cambridge, 2004).
- [15] G. Casella and R. L. Berger, *Statistical Inference*, 2nd ed. (Duxbury Press, Pacific Grove, CA, 2002) reprinted by Duxbury Resource Center, 2006.
- [16] M. C. de Oliveira, Characterization and quantification of symmetric gaussian-state entanglement through a local classicality criterion, *Phys. Rev. A* **72**, 012317 (2005).
- [17] Similar behavior is observed by F_{22} related to inference of $n_2(0)$, not shown due to symmetry with F_{11} .
- [18] A. Serafini, F. Illuminati, M. G. Paris, and S. De Siena, Quantum continuous-variable systems: Characterization and entanglement, *Journal of Physics B: Atomic, Molecular and Optical Physics* **37**, L21 (2004).
- [19] R. Simon, Peres-horodecki separability criterion for continuous variable systems, *Physical Review Letters* **84**, 2726 (2000).
- [20] M. C. de Oliveira, p -representable subset of all bipartite gaussian separable states, *Phys. Rev. A* **70**, 034303 (2004).
- [21] M. C. de Oliveira, F. Nicacio, and S. S. Mizrahi, Minkowski structure for purity and entanglement of gaussian bipartite states, *Phys. Rev. A* **88**, 052324 (2013).